

Iridium(III) Complexes Bearing a Formal Tetradentate Coordination Chelate: Structural Properties and Phosphorescence Fine-Tuned by Ancillaries

Yi Yuan,^{†,‡} Premkumar Gnanasekaran,[§] Yu-Wen Chen,[§] Gene-Hsiang Lee,^{||} Shao-Fei Ni,[⊥] Chun-Sing Lee,^{†,‡,*} and Yun Chi^{†,§,*}

[†]Department of Materials Science and Engineering, Department of Chemistry, City University of Hong Kong, Hong Kong SAR, China

[‡]Center of Super-Diamond and Advanced Films (COSDAF), City University of Hong Kong, Hong Kong SAR, China

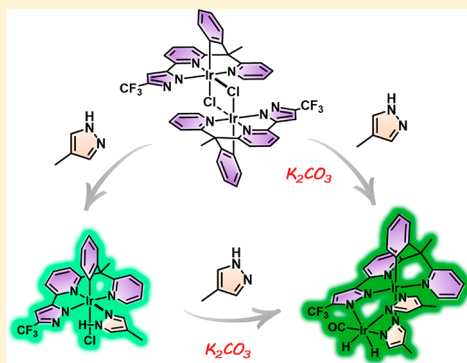
[§]Department of Chemistry and Frontier Research Center on Fundamental and Applied Sciences of Matters, National Tsing Hua University, Hsinchu 30013, Taiwan

^{||}Instrumentational Center, National Taiwan University, Taipei 10617, Taiwan

[⊥]Department of Chemistry, Southern University of Science and Technology, Shenzhen 518055, China

Supporting Information

ABSTRACT: Synthesis of the multidentate coordinated chelate N3C–H₂, composed of a linked functional pyridyl pyrazole fragment plus a peripheral phenyl and pyridyl unit, was obtained using a multistep protocol. Preparation of Ir(III) metal complexes bearing a N3C chelate in the tridentate (κ^3), tetradentate (κ^4), and pentadentate (κ^5) modes was executed en route from two nonemissive dimer intermediates [Ir(κ^3 -N3CH)Cl₂]₂ (1) and [Ir(κ^4 -N3C)Cl]₂ (2). Next, a series of mononuclear Ir(III) complexes with the formulas [Ir(κ^4 -N3C)Cl(py)] (3), [Ir(κ^4 -N3C)Cl(dmap)] (4), [Ir(κ^4 -N3C)Cl(mpzH)] (5), and [Ir(κ^5 -N3C)Cl(dmpzH)] (6), as well as diiridium complexes [Ir₂(κ^5 -N3C)(mpz)₂(CO)(H)₂] (7) and [Ir₂(κ^5 -N3C)(dmpz)₂(CO)(H)₂] (8), were obtained upon treatment of dimer 2 with pyridine (py), 4-dimethylaminopyridine (dmap), 4-methylpyrazole (mpzH), and 3,5-dimethylpyrazole (dmpzH), respectively. These Ir(III) metal complexes were identified using spectroscopic methods and by X-ray crystallographic analysis of representative derivatives 3, 5, and 7. Their photophysical and electrochemical properties were investigated and confirmed by the theoretical simulations. Notably, green-emitting organic light-emitting diode (OLED) on the basis of Ir(III) complex 7 gives a maximum external quantum efficiency up to 25.1%. This result sheds light on the enormous potential of this tetradentate coordinated chelate in the development of highly efficient iridium complexes for OLED applications.



INTRODUCTION

A great deal of current research has been focused on both the designs and applications of emissive, third-row transition metal complexes bearing various bidentate and multidentate coordination chelates.^{1–9} In contrast to the complexes bearing only bidentate chelates, it is believed that the multidentate chelates are capable of increasing the ligand field stabilization energy and inhibiting chelate dissociation, affording emitters with higher emission quantum efficiency and enhanced stability under severe conditions. Given the wide application of transition-metal-based emitters in the fabrication of organic light-emitting diodes (OLED), particular emphasis has been placed on elucidating the roles these multidentate chelates may play in improving the photophysical properties and on how they are going to affect the chemistry and reactivity.¹⁰ Among the plethora of molecular designs, a large variety of Ir(III) and Pt(II) phosphors bearing at least one tridentate chelate have

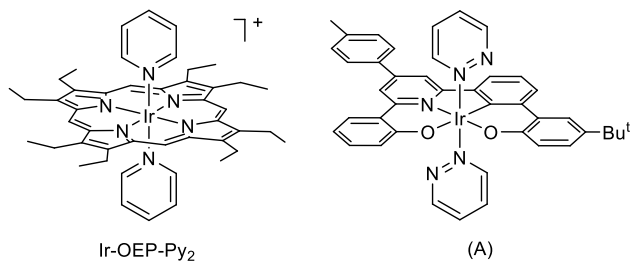
been reported,^{4,11–13} especially in the fabrication of OLED, with performances comparable to those of metal phosphors assembled using traditional bidentate chelates. It should be further emphasized that there is also a class of Ir(III) phosphors with two tridentate chelates, i.e., the so-called bis-tridentate Ir(III) phosphors,^{14–17} and it has showed great promise for OLED fabrication due to both the higher rigidity and stability imposed by their dual tridentate framework.

Hence, the surge in employing multidentate chelate has led to the design of tetradentate chelate and the preparation of emissive Ir(III) or Pt(II) metal phosphors.^{18–22} Furthermore, tetradentate chelates, in comparison to the tridentate chelate of octahedral complexes, are anticipated to have an even better capability in encapsulating the central metal ion and forming

Received: September 19, 2019

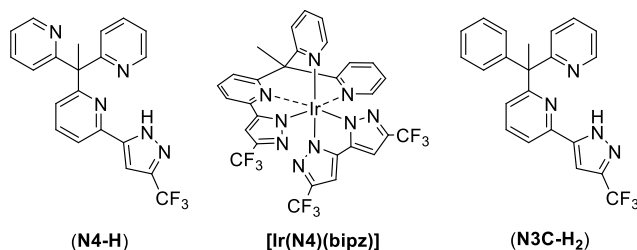
well-defined environments. Hence, they have been thoroughly examined for fundamental studies to serve as the durable template in the construction of redox mediators²³ or catalysts for the activation of small molecules.^{24–28} However, as for the application in making emissive metal complexes, it is essential to introduce some conjugated segment into the chelate backbone to allow systematic fine-tuning of the $\pi\pi^*$ energy gap and emission hue. To account for this requirement, porphyrin-based chelates were known to afford red to NIR-emitting Ir(III) complexes, such as Ir-OEP-Py₂, due to the extended conjugation (Chart 1).²⁹ A second example involved

Chart 1. Structural Drawings of Ir-OEP-Py₂ and (A)



a series of Ir(III) complexes represented by (A), with a planar tetradentate chelate and two axial ancillaries, which has been applied in making the solution-processed red-emitting OLED devices with an external quantum efficiency (EQE) of 10.5%.³⁰ Moreover, a distinctive facially arranged tetradentate 2,2'-(1-(6-(3-trifluoromethyl-1H-pyrazol-5-yl)pyridin-2-yl)ethane-1,1-diyl)dipyridine chelate (e.g., N4–H in Chart 2)³¹ was also

Chart 2. Structural Drawings of Two Tetradentate Chelates N4–H and N3C–H₂ and Ir(III) Metal Complex [Ir(N4)(bipz)]



successfully obtained and put in the preparation of emissive Ir(III) metal complexes. Unlike its planar counterpart, this class of chelate would retain a pair of vacant *cis*-coordination sites for accommodating a bidentate chelate, giving Ir(III) complexes with a novel 4 + 2 architecture. This chemical transformation was evidenced by the addition of di-(trifluoromethyl)-3,3'-bipyrazolate giving a charge-neutral, sky-blue emitting Ir(III) complex [Ir(N4)(bipz)].³¹

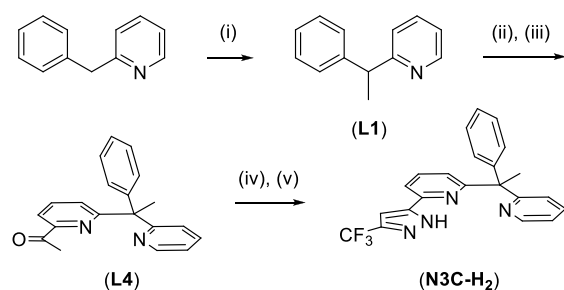
Herein, we present the structural design and characterization of emissive Ir(III) complexes composed of a new class of tetradentate chelate, which differs from previously reported N4–H by replacing one peripheral pyridine with a phenyl substituent, giving 2-(3-trifluoromethyl-1H-pyrazol-5-yl)-6-(1-phenyl-1-(pyridin-2-yl)ethyl)pyridine, cf. N3C–H₂ in Chart 2. This tetradentate chelate is expected to impose a large alternation in electronic properties, as the phenyl group would engage in cyclometalation rather than simple coordination as expected for a pyridyl group. Moreover, this newly

designed N3C–H₂ chelate would act as the dianionic chelate, which is in sharp contrast to the monoanionic behavior exhibited by N4–H, not to mention that the cyclometalation requires a higher activation barrier as well as the production of distinctive intermediate species. Hence, we are interested in probing the structure–property relationship of relevant Ir(III) complexes. After that, we are also interested in studying the mechanistic information en route to the isolation of novel diiridium dihydride complexes, via pyrazole coordination in the presence of K₂CO₃. Eventually, the removal of the remaining chloride and monodentate N-donor have produced the metal complexes with much enhanced photoluminescence.

RESULTS AND DISCUSSION

Syntheses and Characterization. The dianionic chelate N3C–H₂ described in this paper was prepared using 1-phenyl-1-(pyridin-2-yl)ethane (L1), which was obtained by direct methylation of commercially available 2-benzylpyridine (Scheme 1). Independently, 2-bromo-6-(2-methyl-1,3-dioxo-

Scheme 1. Synthesis of Tetradentate Chelate N3C–H₂^a



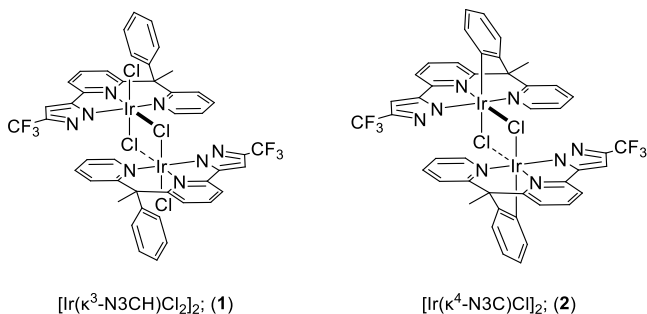
^aExperimental conditions: (i) *n*-BuLi, MeI, THF, –78 °C. (ii) *n*-BuLi, 2-bromo-6-(2-methyl-1,3-dioxolan-2-yl)pyridine, THF, –78 °C. (iii) HCl, H₂O, reflux. (iv) NaOEt, CF₃CO₂Et, THF, reflux. (v) N₂H₄·H₂O, conc HCl, EtOH, reflux.

lan-2-yl)pyridine was prepared from the treatment of 2,6-dibromopyridine with *n*-BuLi, followed by the addition of dimethylacetamide and the protection of the acetyl group by treatment with ethylene glycol in the presence of *p*-toluenesulfonic acid. After that, the coupling of 1-phenyl-1-(pyridin-2-yl)ethane with 2-bromo-6-(2-methyl-1,3-dioxolan-2-yl)pyridine, followed by acid catalyzed hydrolysis, afforded the key intermediate 1-(6-(1-phenyl-1-(pyridin-2-yl)ethyl)pyridin-2-yl)ethan-1-one (L4) in good yield. Finally, condensation of L4 with ethyl trifluoroacetate, followed by hydrazine cyclization, afforded the desired tetradentate chelate (N3C–H₂). The corresponding synthetic protocol is depicted in Scheme 1.

Next, this tetradentate chelate N3C–H₂ was reacted with an iridium reagent IrCl₃·3H₂O using a two-step coordination pattern. These manipulations led to the isolation of two distinctive Ir(III) complexes, [Ir(κ^3 -N3CH)Cl₂]₂ (1) and [Ir(κ^4 -N3C)Cl]₂ (2), from reactions conducted either in mixed 2-methoxyethanol (bp = 124 °C) and water or in refluxing diethylene glycol monomethyl ether (DGME, bp = 194 °C), respectively. The key data to their assignment is provided by their ¹H NMR spectra, which exhibited a total of 13 and 12 proton signals in the aromatic region, together with a distinctive high-field methyl signal at δ 2.25 and δ 2.82 of N3C chelate. The spectral pattern also confirmed the presence of a free rotating phenyl appendage in 1 in solution and a

rigidified cyclometalate phenyl group of the second dimer intermediate 2. Besides, only the powders can be obtained for both complexes, despite multiple attempts in conducting crystallization and with distinctive solvents, which hampered characterization using single crystal X-ray diffraction analysis. This could be due to the existence of two possible isomers in forming the proposed dimer complexes, i.e., *cis* and *trans* forms, in both solution and solid states. However, only the structural drawings of the *trans* isomer are depicted in Chart 3 for conveying our assignments.

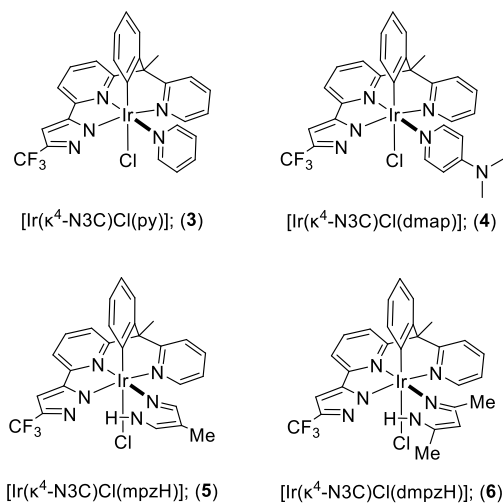
Chart 3. Drawings of Dimeric Intermediates 1 and 2 in *Trans* Arrangement



Relevant diiridium metal complexes with bridged chloride ligands were known to undergo facile addition of the donor group to afford the mononuclear metal complexes;^{32–36} hence, the diiridium metal complex 2 should be of no exception. To confirm this speculation, we attempted the reactions with various nitrogen donors, namely, pyridine (py), 4-dimethylaminopyridine (dmap), 4-methylpyrazole (mpzH), and 3,5-dimethylpyrazole (dmpzH) from which we obtained mononuclear Ir(III) complexes, namely, $[\text{Ir}(\kappa^4\text{-N3C})\text{Cl}(\text{py})]$ (3), $[\text{Ir}(\kappa^4\text{-N3C})\text{Cl}(\text{dmap})]$ (4), $[\text{Ir}(\kappa^4\text{-N3C})\text{Cl}(\text{mpzH})]$ (5), and $[\text{Ir}(\kappa^4\text{-N3C})\text{Cl}(\text{dmpzH})]$ (6) in moderate yields (cf. Chart 4). The initial identification was provided by their FD MS data that exhibited the anticipated molecular ion (M^+) and their ¹H NMR spectra with all proton signals for both the N3C chelate and added nitrogen donor in a 1:1 ratio.

Single crystal X-ray diffraction studies on 3 and 5 were next conducted to reveal their structural characteristics. As shown in

Chart 4. Drawings of Mononuclear Ir(III) Complexes 3–6



Figures 1 and 2, both molecules exhibit a slightly distorted octahedral arrangement around the iridium atom with the

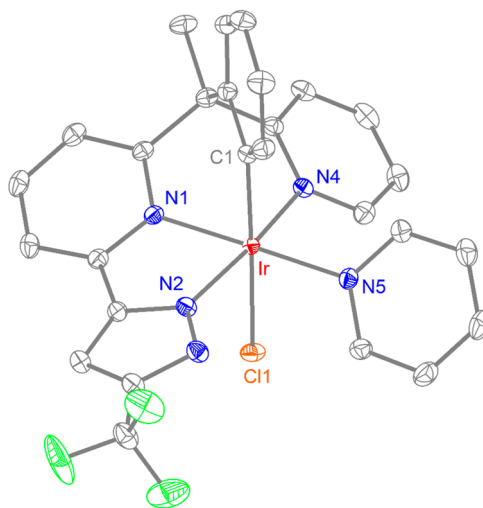


Figure 1. Structure of 3 with thermal ellipsoids shown at the 40% probability, Ir–C(1) = 2.005(4), Ir–N(1) = 2.007(3), Ir–N(2) = 2.021(3), Ir–N(4) = 2.045(3), Ir–N(5) = 2.067(3), and Ir–Cl(1) = 2.4982(9) Å. Selected bond angles: N(2)–Ir–N(4) = 169.44(12), N(1)–Ir–N(5) = 175.24(12), and C(1)–Ir–Cl(1) = 173.35(11)°.

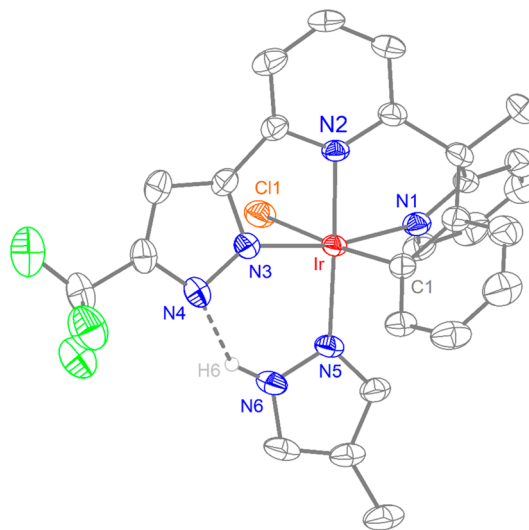


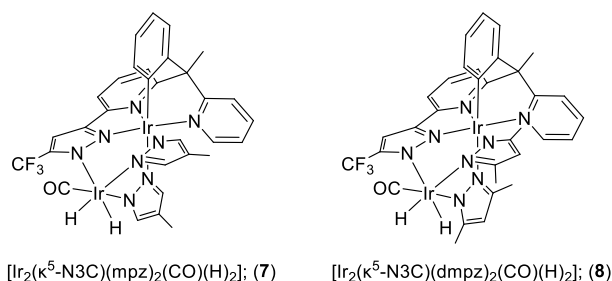
Figure 2. Structure of 5 with thermal ellipsoids shown at the 40% probability, Ir–C(1) = 2.015(5), Ir–N(1) = 2.047(4), Ir–N(2) = 2.005(4), Ir–N(3) = 2.012(4), Ir–N(5) = 2.052(4), and Ir–Cl(1) = 2.4658(13) Å. Selected bond angles: N(1)–Ir–N(3) = 167.50(16), N(2)–Ir–N(5) = 173.34(17), and C(1)–Ir–Cl(1) = 174.24(15)°.

N3C chelate adopting the anticipated tetradentate κ^4 -mode. The pyrazolate-to-central pyridine unit is slightly bent away from planarity to allow the coordination of peripheral phenyl and pyridyl units. Overall, the three N atoms of N3C chelates are arranged in the meridional mode, while the phenyl appendage is located at the axial site vs the plane defined by the meridional arranged N atoms and is located at the *trans* disposition to the unique chloride, leaving the monodentate N donor to occupy the remaining coordination site that is *trans* to the central pyridine unit of N3C chelate. The unique Ir–C distances of 2.005(4) Å in 3 and 2.015(5) Å in 5 are similar to the reported Ir–C bond distances *trans* to the chloride,³⁷ while

the py and mpzH ligands of **3** and **5** exhibited the longest Ir–N distances within each molecule, i.e., 2.067(3) and 2.052(4) Å, which could be due to the strong *trans* influence exerted by the central pyridine unit of the N3C chelate, which exhibited the shortest Ir–N distance, i.e., 2.007(3) and 2.005(4) Å. Finally, the monodentate pyridine in **3** is rotated along the N–Ir vector by $\sim 45^\circ$ for minimizing steric interaction to the nearby pyrazolate fragment of the N3C chelate. In sharp contrast, the mpzH ligand in **5** is aligned parallel to this pyrazolate to allow for the formation of interligand H-bonding, i.e., with N(4)⋯H(6)–N(6) contact of 1.990 Å. This observation is also consistent with the downfield-shifted pyrazolic proton signal at δ 14.20 in its ^1H NMR spectrum recorded in CD_2Cl_2 solvent at room temperature (RT).

We next conducted the reaction of **2** with pyrazoles under basic conditions, with an anticipation that the pyrazolate is capable of replacing the chloride anion, giving dinuclear complexes connected with two bridging pyrazolates.^{38–47} To our surprise, when the mixture of **2**, mpz/dmpz (8 equiv), and K_2CO_3 (5 equiv) was refluxed in DGME for 12 h, these reactions went in a different direction and afforded the diiridium metal complexes $[\text{Ir}_2(\kappa^5\text{-N3C})(\text{mpz})_2(\text{CO})(\text{H})_2]$ (**7**) and $[\text{Ir}_2(\kappa^5\text{-N3C})(\text{dmpz})_2(\text{CO})(\text{H})_2]$ (**8**) as shown in Chart 5, for which their ^1H NMR spectra exhibited two

Chart 5. Structural Drawings of Diiridium Complexes 7 and 8



hydride signals at δ –16.70 and δ –19.73 and δ –16.66 and δ –19.75 and IR spectra displayed a characteristic $\nu(\text{CO})$ stretching band at 2011 and 2007 cm^{-1} , respectively. For the hydride signals in ^1H NMR spectra, one appears as a doublet with $^2J_{\text{HH}}$ of ~ 8.3 Hz, which is caused by the mutual coupling of *cis*-oriented hydrides, while the second multiplet, with an additional, smaller coupling constant of $^5J_{\text{HF}} = \sim 3.8$ Hz, is attributed to the long-range (or through space) coupling to an adjacent CF_3 substituent. Since this spectroscopic information cannot unambiguously identify their molecular arrangements, a single crystal X-ray structural determination on **7** was next conducted to decipher their exact structure.

The single crystal X-ray structural analysis on **7** depicted the existence of two crystallographically independent, but structurally similar, molecules within the unit cells. Figure 3 shows one molecular drawing of these molecules, which consists of one pentacoordinated $\kappa^5\text{-N3C}$ chelate spanning across two octahedral arranged Ir(III) metal centers. The first Ir(1) metal atom interacts with the N3C chelate using the κ^4 -mode, while the remaining *cis*-coordination sites are bridged by two mpz chelates. These three pyrazolate chelates, one from N3C and two from mpz anions, formed a facially coordinated tridentate ensemble, in a manner related to that of the well-established tris-pyrazolyl borate chelates known to the coordination chemistry,^{48–50} and interacted with the second

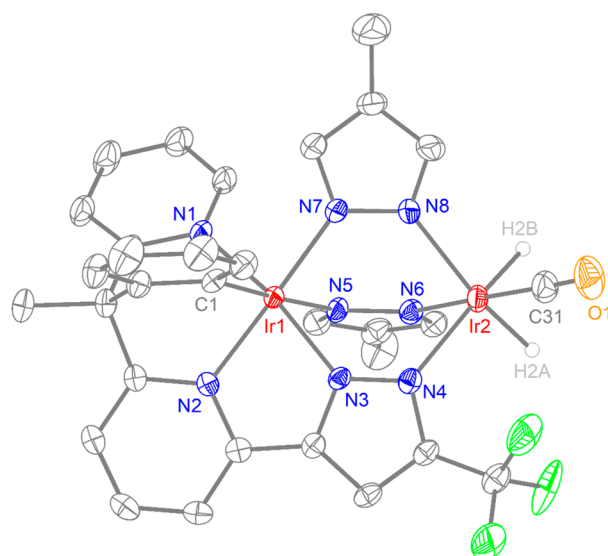


Figure 3. Structure of **7** with thermal ellipsoids shown at the 40% probability, Ir(1)–C(1) = 2.025(5), Ir(1)–N(1) = 2.039(4), Ir(1)–N(2) = 2.032(4), Ir(1)–N(3) = 2.029(4), Ir(1)–N(5) = 2.158(4), Ir(1)–N(7) = 2.036(4), Ir(2)–C(31) = 1.823(7), Ir(2)–N(4) = 2.210(4), Ir(2)–N(6) = 2.106(4), Ir(2)–N(8) = 2.137(4), Ir(2)–H(2A) = 1.52(6), and Ir(2)–H(2B) = 1.547(10) Å. Selected bond angles: N(1)–Ir1–N(3) = 166.48(17), N(2)–Ir1–N(7) = 171.23(17), N(5)–Ir1–C(1) = 177.68(18), and N(6)–Ir2–C(31) = 172.3(2) $^\circ$.

Ir(2) metal center. The three remaining coordination sites on Ir(2) are next occupied by two *cis*-arranged hydrides and a terminal carbonyl. Other metric parameters within this molecule are normal and unremarkable.

As for a possible reaction pathway, the hydrides of both **7** and **8** may be derived from the hydroxyl group of a protic solvent employed in the present studies, for which the employed conditions are akin to many transformations documented in the literature.^{51,52} We have also tried to confirm this possibility by using isotope tracing, i.e., the addition of D_2O into the reaction mixture. However, the introduction of a small amount of D_2O has failed to incorporate enough deuteride in the final product, but too much D_2O caused a complete suppression of product formation, giving no answer to their origins. On the contrary, the carbonyl group of both **7** and **8** is attributed to the added K_2CO_3 catalyst. As shown in Figure S1, in contrast to the formation of diiridium complex **7** with only one $\nu(\text{CO})$ stretching band at 2011 cm^{-1} , the addition of 10 and 25 equiv of ^{13}C -isotope enriched K_2CO_3 afforded diiridium complex **7** with an additional $\nu(\text{CO})$ stretching signal at 1965 cm^{-1} . Hence, some of the carbonate ion dissolved in the reaction media has been reduced by forming carbon monoxide in the reaction media and, eventually, participating in the formation of the diiridium products. Moreover, the heating of Ir(III) complexes **5** and **6** with a corresponding pyrazole in the presence of K_2CO_3 also afforded the diiridium complexes **7** and **8** in lower yields, which confirmed the possible intermediacy of mononuclear **5** and **6** while the lower yields reflected the demand of a second Ir(III) metal fragment en route to the formation of diiridium complexes **7** and **8**.

Photophysical Properties. The diiridium complexes **1** and **2** are essentially nonemissive in both solution and solid states, and hence, only the photophysical data of Ir(III)

complexes 3–8 were recorded and depicted in Figure 4, while their numeric data were summarized in Table 1. In general, all

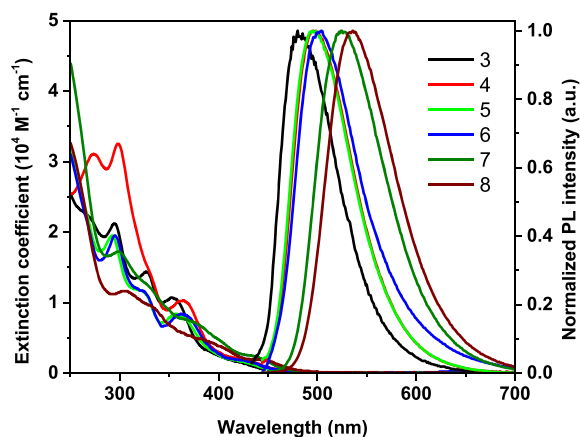


Figure 4. UV-vis absorption and emission of Ir(III) complexes in CH_2Cl_2 solution at 10^{-5} M at RT.

higher energy absorption peaks (≤ 400 nm) with higher excitation coefficients in UV-vis spectra are attributed to the intraligand charge transfer (ILCT) transition of tetradentate κ^4 -N3C chelate. Moreover, the strong absorption of 4 at approximately 298 nm originates from the charge transfer absorption of coordinated 4-dimethylaminopyridine. Finally, the absorptions at ~ 420 nm and their shoulder in the lower energy region ≥ 470 nm are attributed to both the spin allowed and forbidden metal-to-ligand charge transfer (MLCT) transition.

As for the emission, all studied Ir(III) complexes showed a broadened, structureless profile with a peak maximum between 480–505 nm for Ir(III) complexes 3–6 and at 524 and 536 nm for diiridium complexes 7 and 8, respectively. It is notable that complexes 3–6 exhibited poor emission quantum yields (QY), which are due to the fast nonradiative process exerted by both the weak-field chloride ligand and monodentate nitrogen donor. In sharp contrast, the diiridium complexes 7 and 8 exhibited much higher QY due to the absence of chloride and the possession of two bridging pyrazolates; the latter would allow a significantly reduced rotational freedom in solution in comparison to the case for the monodentate coordinated pyridines or pyrazoles.

Thermal and Electrochemical Properties. The thermal properties of the titled complexes 3–8 were evaluated by thermal gravimetric analysis under a nitrogen atmosphere. As depicted in Figure S2, the decomposition temperature with a 5% weight loss for complexes 3–8 was recorded in the range 287–389 °C, indicating their good thermal stability.

The oxidation and reduction potentials of 3–8 were measured by cyclic voltammetry, to which the data and corresponding voltammograms were depicted in Table 1 and Figure S3. As can be seen, all mononuclear complexes 3–6 showed a quasi-reversible, metal-centered oxidation process, for which those with a more electron donating nitrogen donor, i.e., dmap vs py and dmpzH vs mpzH, displayed a slight shifting of potential to a less positive region, confirming the metal-centered oxidation process. Moreover, dmap-substituted complex 4 exhibited the least positive oxidation potential among all complexes, which could be due to the strongest electron donating effect exerted by the dimethylamino group of dmap ligand. On the contrary, the oxidation peak profile of diiridium complexes 7 and 8 turned irreversible and underwent a slight cathodic shifting at the same time, making the corresponding electrochemistry distinctive from their mononuclear counterparts 3–6. This result echoes the large distinction between mononuclear and diiridium metal complexes. Finally, their HOMO/LUMO energy levels were calculated to be $-5.68/-2.29$, $-5.52/-2.26$, $-5.65/-2.39$, $-5.64/-2.28$, $-5.62/-2.37$, and $-5.54/-2.39$ eV for complexes 3–8, respectively, according to the equation of $\text{HOMO/LUMO} = -(E_{\text{ox}}/E_{\text{red}} + 4.8)$ eV.

Theoretical Investigations. Density functional theory (DFT) and time-dependent DFT (TDDFT) calculations were performed on Ir(III) complexes 3, 5, and 7 in order to decipher their photophysical and electrochemical characteristics. As depicted in Figure 5, both complexes 3 and 5, bearing a monodentate py and a mpzH ligand, have similar HOMO distributions, with electron clouds mainly located on the central iridium atom, chloride, and both pyrazolate and phenyl rings of κ^4 -N3C chelate. However, the location of the LUMO is slightly different, for which the electron cloud of 3 is spread over the entire κ^4 -N3C chelate except for the phenyl ring, while for complex 5, the LUMO showed little contribution from the mpzH ancillary, probably due to both the slightly stronger donor strength and the reduced π -conjugation. For the diiridium complex 7, the HOMO is mainly localized on the Ir(1) atom (as defined in single crystal X-ray structural analysis), the phenyl ring of the κ^5 -N3C chelate, and two bridging mpz anions, while the LUMO is primarily dispersed over the pyrazolate and both pyridyl fragments of the κ^5 -N3C chelate as well as the central Ir(1) atom.

Besides, complexes 3, 5, and 7 exhibited the HOMO levels of -5.78 , -5.77 , and -5.76 eV, respectively, which are consistent with their CV data (Figure S3 and Table 1). The associated electronic transitions and emission wavelengths are next calculated on the basis of their optimized S_0 geometries. As depicted in Table S1, the calculated $S_0 \rightarrow S_1$ transition wavelengths for 3 (379.3 nm), 5 (379.74 nm), and 7 (380.18

Table 1. Photophysical and Electrochemical Data of the Studied Ir(III) Metal Complexes

	abs λ [nm] ($\epsilon \times 10^{-4}$ M $^{-1}$ cm $^{-1}$) ^a	λ_{max} (nm) ^a	Φ (%) ^a	τ_{obs} (μ s) ^a	k_{r} (s $^{-1}$)	k_{nr} (s $^{-1}$)	E_{ox} [V] ^b	E_{red} [V] ^b
3	294 (2.12), 326 (1.44), 353 (1.07)	480	0.86	0.011	7.8×10^5	9.0×10^7	0.88	−2.51
4	273 (3.11), 298 (3.25), 364 (1.03)	496	1.5	0.041	3.7×10^5	2.4×10^7	0.72	−2.54
5	292 (1.95), 320 (1.17), 358 (0.83)	495	1.2	0.032	3.8×10^5	3.1×10^7	0.85	−2.41
6	295 (1.95), 319 (1.19), 362 (0.84)	504	1.2	0.014	8.6×10^5	7.1×10^7	0.84	−2.52
7	299 (1.72), 365 (0.76), 436 (0.23)	524	75	5.96	1.3×10^5	4.2×10^4	0.82	−2.43
8	305 (1.16), 381 (0.49), 440 (0.19)	536	72	6.96	1.0×10^5	4.0×10^4	0.74	−2.41

^aUV-vis spectra, PL spectra, and lifetime and quantum yields were recorded in CH_2Cl_2 at a concentration of 10^{-5} M at RT. ^bThe oxidation and reduction potentials were recorded in CH_2Cl_2 and THF, respectively.

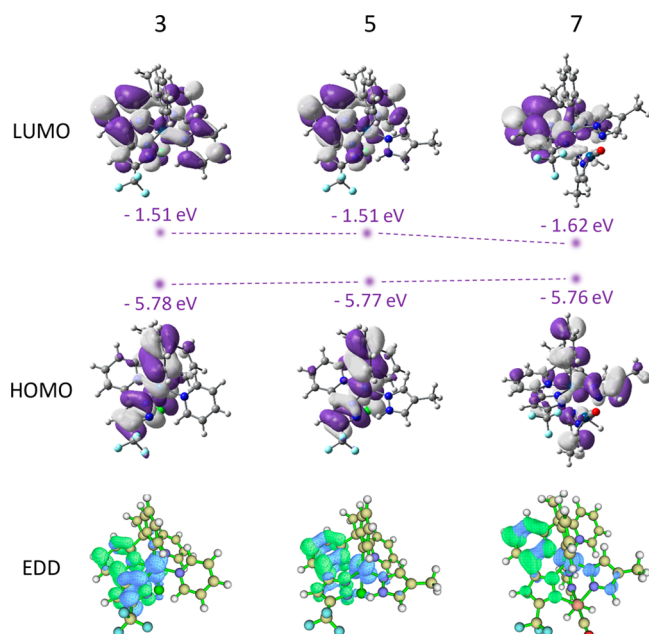


Figure 5. Contours and energy levels of the frontier molecular orbitals in the optimized S_0 state and the electron density difference maps for Ir(III) complexes 3, 5, and 7, to which the blue and green contours of EDD maps represent the decrease and increase of the electron density upon excitation, respectively.

nm) are qualitatively akin to the lowest energy absorption band (Figure 4). The $T_1 \rightarrow S_0$ transition energy was calculated to be 510.47, 574.21, and 585.41 nm for 3, 5, and 7, respectively, showing the same trend to the observed phosphorescence as revealed in Figure 4. As for their assignment, the $S_0 \rightarrow S_1$ and $S_0 \rightarrow T_1$ transitions are both dominated by HOMO-1 \rightarrow LUMO for 3 and HOMO \rightarrow LUMO for 7, respectively, and are changed to HOMO \rightarrow LUMO and HOMO-1 \rightarrow LUMO processes for 5. Also, as depicted in Table S1, their lowest triplet excited states showed mixed MLCT, ILCT, and ligand-to-ligand charge transfer (LLCT) characters. To obtain a clear orbital representation, we applied the electron density difference (EDD) maps to visualize the electronic transition that constituted the lowest triplet excited states. As exhibited in

Figure 5, the negative regions were mainly localized over the central Ir(III) atom and the N3C chelate, and partially on the chloride and monodentate ligands, while the positive areas were distributed over the N3C chelate, indicating the mixed charge transfer transition characteristics.

Fabrication of OLED Devices. Given its high phosphorescence quantum yield, diiridium complex 7 is selected as a representative dopant emitter to investigate its electroluminescent (EL) performance. Thus, the OLEDs with an architecture of indium tin oxide (ITO)/1,1-bis[4-[*N,N'*-di(*p*-tolyl)amino]phenyl]cyclohexane (TAPC, 50 nm)/10 wt % 7 doped in 4,4',4''-tris(*N*-carbazolyl)-triphenylamine (TCTA, 20 nm)/3,3'-(5'-(3-(pyridin-3-yl)-phenyl)-[1,1':3',1''-terphenyl]-3,3''-diyl)dipyridine (TmPyPB, 50 nm)/LiF (1 nm)/Al (120 nm) was fabricated. Doped TCTA constituted the light-emissive layer (EML), while TAPC and TmPyPB served as the hole-transporting and electron-transporting layers, respectively. As shown in Figure 6, this device gives bright green emission with a peak maximum at 530 nm and CIE 1931 chromaticity coordinates of (0.34, 0.59). The EL spectrum is essentially identical to its solution PL spectrum and free from the TCTA host emission and others, indicating the efficient energy transfer and exciton confinement within the EML. As shown in the current density–voltage–luminance (J – V – L) curve, this device exhibited a small charge injection barrier by giving low turn-on voltage of <3.5 V at a brightness of 1 cd m^{-2} . Figure 6b shows the device efficiency at different current densities, for which an excellent performance with a maximum current efficiency of 81.7 cd A^{-1} and external quantum efficiency of 25.1% were obtained. Moreover, upon an increase in the luminance to 1000 cd m^{-2} , its EQE remains as high as 20%. These device performances are much better than our previous report on the Ir(III) emitter bearing tetradentate N4 chelate,³¹ albeit with a much red-shifted emission wavelength. Unfortunately, like most reported phosphorescent OLED devices, as the luminance or current density is further increased, the efficiency dropped rapidly, which can be explained by triplet–triplet annihilation caused by the relatively long lifetime of Ir(III) dopant 7. Further optimization targeted at increasing the optical bandgap of the N3C-based Ir(III) complex is under way.

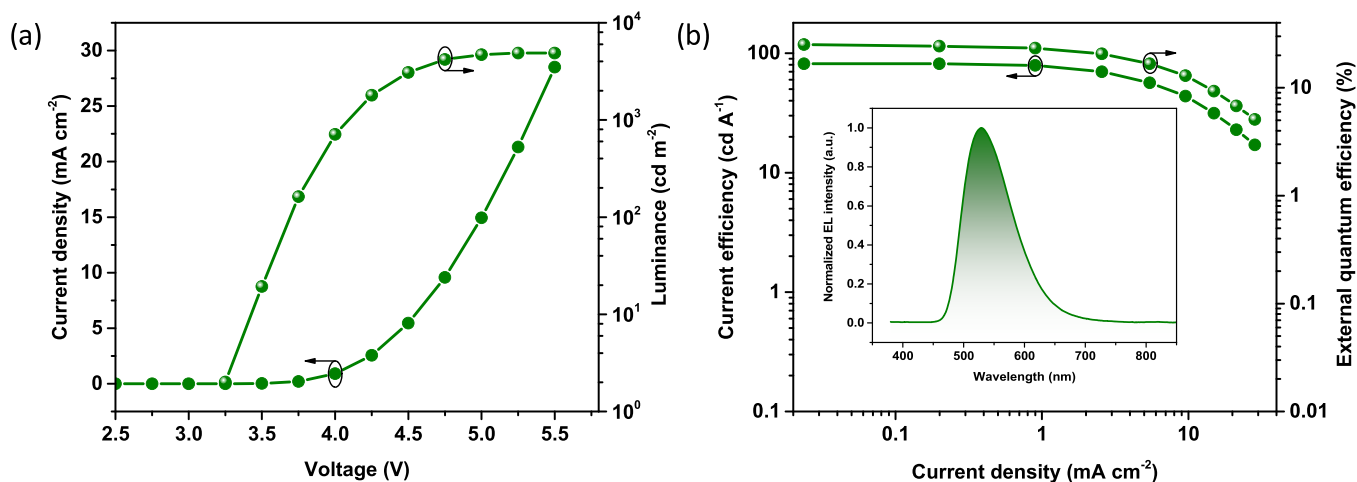


Figure 6. (a) Current density–voltage–luminance (J – V – L) characteristics and (b) efficiency versus current density plots for complex-7-based OLEDs (inset: EL spectra at 4.5 V).

CONCLUSION

In summary, we designed and synthesized a potentially tetradentate coordinated chelate, namely, 2-(3-trifluoromethyl-1*H*-pyrazol-5-yl)-6-(1-phenyl-1-(pyridin-2-yl)ethyl)pyridine (N3C-H₂). A series of mononuclear and diiridium metal complexes were next obtained with the N3C chelate, showing a metal–ligand bonding mode varying from a κ^3 -mode in dimer **1** to a κ^4 -mode in both dimer **2** and mononuclear Ir(III) complexes **3–6** and finally to a κ^5 -mode in diiridium complexes **7** and **8**, respectively. The mechanistic pathways that give these Ir(III)-based metal complexes were unambiguously clarified. Except for dimer complexes **1** and **2**, which are essentially nonemissive, other newly synthesized mononuclear complexes **3–6** and diiridium complexes **7** and **8** exhibited bright sky-blue to green emissions with a peak wavelength spanning 480–536 nm. More importantly, the removal of the chloride and monodentate ancillary produced the diiridium complexes **7** and **8** with much enhanced emission efficiency. Therefore, the green OLEDs incorporating **7** as the dopant emitter achieved excellent performance with an emission peak maximum located at 530 nm and with a maximum EQE of 25.1% and luminescence of 81.7 cd A⁻¹. Hence, our study presents a new approach in designing efficient iridium-based phosphors for OLED applications.

EXPERIMENTAL SECTION

General Information and Materials. All reactions were performed under a nitrogen atmosphere. Solvents were distilled from appropriate drying agents prior to use. Commercially available reagents were used without further purification. Mass spectra were obtained on a JEOL AccuTOF GCX instrument operating in field desorption (FD) mode. ¹H and ¹⁹F NMR spectra were obtained using the Varian Mercury-400 and -500 NMR instruments. Elemental analyses were performed using the Elementar Vario EL III CHN-O rapid elementary analyzer. Steady-state absorption and emission spectra were recorded by a Hitachi (U-3900) spectrophotometer and an Edinburgh (FLS920) fluorometer, respectively. To determine the photoluminescence quantum yield in solution, the samples were degassed by three freeze–pump–thaw cycles. All electrochemical potentials were measured in a 0.1 M TBAPF₆/CH₂Cl₂ solution for oxidation and THF for reduction reaction and were reported in volts using Fc/Fc⁺ as the reference; ΔE_p is defined as E_{pa} (anodic peak potential) – E_{pc} (cathodic peak potential), and these data are quoted in millivolts. Platinum and gold wires were selected as the cathode and anode of electrochemical measurements, respectively.

Preparation of [Ir(κ^3 -N3CH)Cl₂]₂ (1**).** A mixture of IrCl₃·3H₂O (200 mg, 0.57 mmol) and N3C-H₂ (0.22 g, 0.56 mmol) in 30 mL of 2-methoxyethanol and 10 mL of water was refluxed for 12 h. After it cooled to RT, the resulting precipitate was collected and washed with ethanol and diethyl ether to afford light-yellow solid **1** (290 mg, 76%).

Spectral data of **1**. ¹H NMR (400 MHz, DMSO-*d*₆, 298 K): δ 10.57 (d, *J* = 5.8 Hz, 1H), 7.86 (d, *J* = 7.6 Hz, 1H), 7.68 (t, *J* = 7.5 Hz, 1H), 7.61 (t, *J* = 7.9 Hz, 1H), 7.40 (m, 4H), 7.33–7.27 (m, 2H), 7.19 (s, 1H), 7.02 (d, *J* = 8.1 Hz, 1H), 6.71 (d, *J* = 8.1 Hz, 1H), 2.25 (s, 3H). ¹⁹F NMR (376 MHz, DMSO-*d*₆, 298 K): δ –58.42 (s, 3F). FD MS: *m/z* 1205.1 (M⁺ – H₂Cl₃). Anal. Calcd for C₄₄H₃₂Cl₄F₆Ir₂N₈: C, 40.25; H, 2.46; N, 8.53. Found: C, 39.87; H, 2.81; N, 8.73.

Preparation of [Ir(κ^4 -N3C)Cl]₂ (2**).** A mixture of **1** (290 mg, 0.22 mmol) in 20 mL of diethylene glycol monomethyl ether (DGME) was refluxed for 12 h. After it cooled to RT, the solvent was removed and the residue was taken into CH₂Cl₂, washed with water, dried over Na₂SO₄, filtered, and concentrated to dryness. It was purified by silica gel column chromatography (CH₂Cl₂ and methanol = 10:1) to afford light-yellow solid **2** (210 mg, 76%).

Spectral data of **2**. ¹H NMR (400 MHz, CD₂Cl₂, 298 K): δ 9.46 (d, *J* = 4.5 Hz, 1H), 8.22–8.15 (m, 2H), 8.03 (t, *J* = 6.4 Hz, 1H), 7.90–

7.88 (m, 2H), 7.56 (t, *J* = 5.2 Hz, 1H), 7.53 (d, *J* = 6.2 Hz, 1H), 7.43 (d, *J* = 6.3 Hz, 1H), 7.07 (t, *J* = 6.0 Hz, 1H), 6.98 (t, *J* = 5.9 Hz, 1H), 6.78 (s, 1H), 2.82 (s, 3H). ¹⁹F NMR (376 MHz, CD₂Cl₂, 298 K): δ –60.45 (s, 3F). FD MS: *m/z* 1205.1 (M⁺ – Cl). Anal. Calcd for C₄₄H₃₀Cl₂F₆Ir₂N₈: C, 42.62; H, 2.44; N, 9.04. Found: C, 42.35; H, 2.24; N, 9.59.

Preparation of [Ir(κ^4 -N3C)Cl(py)] (3**).** A mixture of **2** (300 mg, 0.24 mmol) and pyridine (py, 153 mg, 1.93 mmol) in 40 mL of DGME was refluxed for 14 h. After it cooled to RT, the solvent was removed and the residue was taken into CH₂Cl₂, washed with water, dried over Na₂SO₄, filtered, and concentrated to dryness. It was purified by silica gel column chromatography (CH₂Cl₂ and ethyl acetate = 3:1) to afford light-yellow solid [Ir(κ^4 -N3C)Cl(py)] (**3**, 140 mg, 41%).

Spectral data of **3**. ¹H NMR (500 MHz, DMSO-*d*₆, 373 K): δ 8.62 (s, 2H), 8.17–8.02 (m, 4H), 7.95 (t, *J* = 7.9 Hz, 1H), 7.78 (d, *J* = 7.6 Hz, 1H), 7.67 (d, *J* = 7.8 Hz, 1H), 7.54 (t, *J* = 6.7 Hz, 2H), 7.35 (d, *J* = 7.7 Hz, 1H), 7.29 (t, *J* = 6.1 Hz, 1H), 7.15 (s, 1H), 6.88 (t, *J* = 7.3 Hz, 1H), 6.82 (d, *J* = 7.1 Hz, 1H), 6.68 (t, *J* = 7.2 Hz, 1H), 2.66 (s, 3H). ¹⁹F NMR (471 MHz, DMSO-*d*₆, 373 K): δ –58.50 (s). FD MS: *m/z* 699.0 (M⁺). Anal. Calcd for C₂₇H₂₀ClF₃IrN₅: C, 46.38; H, 2.88; N, 10.02. Found: C, 46.73; H, 2.57; N, 9.81.

Selected X-ray structural data of **3**: C₂₈H₂₂Cl₃F₃IrN₅; *M* = 784.08; triclinic; space group = $P\bar{1}$, *a* = 9.5645(3) Å, *b* = 12.3522(4) Å, *c* = 14.4243(4) Å; α = 107.7491(9)°, β = 97.3463(9)°, γ = 104.0035(9)°; *V* = 1536.83(8) Å³; *Z* = 4; ρ_{calcd} = 1.690 Mg·m⁻³; *F*(000) = 756; crystal size = 0.135 × 0.127 × 0.088 mm³; *T* = 150 (2) K; μ = 4.649 mm⁻¹; 14049 reflections collected, 7044 independent reflections (*R*_{int} = 0.0154), max and min transmission = 0.7456 and 0.6324; restraints/parameters = 25/383, GOF = 1.117, final *R*₁[*I* > 2 σ (*I*)] = 0.0262 and *wR*₂ (all data) = 0.0721; largest diff peak and hole = 1.760 and –0.914 e·Å⁻³.

Preparation of [Ir(κ^4 -N3C)Cl(dmap)] (4**).** A mixture of **2** (500 mg, 0.40 mmol) and 4-dimethylaminopyridine (dmap, 390 mg, 3.2 mmol) in 40 mL of DGME was refluxed for 14 h. After it cooled to RT, the solvent was removed and the residue was taken into CH₂Cl₂, washed with water, dried over Na₂SO₄, filtered, and concentrated to dryness. It was purified by silica gel column chromatography (CH₂Cl₂ and ethyl acetate = 3:1) to afford light-yellow [Ir(κ^4 -N3C)Cl(dmap)] (**4**, 300 mg, 46%).

Spectral data of **4**. ¹H NMR (500 MHz, DMSO-*d*₆, 373 K): δ 8.30 (d, *J* = 5 Hz, 1H), 8.07–8.02 (m, 4H), 7.91 (t, *J* = 7.9 Hz, 1H), 7.74 (d, *J* = 7.5 Hz, 1H), 7.63 (d, *J* = 7.9 Hz, 1H), 7.34–7.26 (m, 2H), 7.12 (s, 1H), 6.98 (dd, *J* = 7.4, 1.2 Hz, 1H), 6.89–6.84 (m, 1H), 6.68 (dd, *J* = 10.9, 3.9 Hz, 3H), 3.08 (s, 6H), 2.64 (s, 3H). ¹⁹F NMR (471 MHz, DMSO-*d*₆, 373 K): δ –58.35 (s). FD MS: *m/z* 742.1 (M + H⁺). Anal. Calcd for C₂₉H₂₅ClF₃IrN₆: C, 46.93; H, 3.40; N, 11.32. Found: C, 47.11; H, 3.37; N, 11.32.

Preparation of [Ir(κ^4 -N3C)Cl(mpzH)] (5**).** A mixture of **2** (500 mg, 0.40 mmol) and 4-methylpyrazole (mpzH, 270 mg, 3.2 mmol) in 40 mL of DGME was refluxed for 14 h. After it cooled to RT, the solvent was removed and the residue was taken into CH₂Cl₂, washed with water, dried over Na₂SO₄, filtered, and concentrated to dryness. It was purified by silica gel column chromatography (CH₂Cl₂ and ethyl acetate = 3:1) to afford light-yellow [Ir(κ^4 -N3C)Cl(mpzH)] (**5**, 260 mg, 46%).

Spectral data of **5**. ¹H NMR (400 MHz, CD₂Cl₂, 298 K): δ 14.20 (br, NH, 1H), 8.90 (d, *J* = 5.9 Hz, 1H), 7.91 (d, *J* = 4.8 Hz, 2H), 7.82 (s, 1H), 7.78 (t, *J* = 7.8 Hz, 1H), 7.51 (d, *J* = 7.9 Hz, 2H), 7.31 (d, *J* = 7.7 Hz, 1H), 7.23–7.21 (m, 1H), 6.99 (s, 1H), 6.90–6.82 (m, 3H), 6.66 (t, *J* = 7.4 Hz, 1H), 2.66 (s, 3H), 2.13 (s, 3H). ¹⁹F NMR (376 MHz, CD₂Cl₂, 298 K): δ –60.67 (s, 3F). FD MS: *m/z* 702.1 (M + H⁺). Anal. Calcd for C₂₆H₂₁ClF₃IrN₆: C, 44.48; H, 3.01; N, 11.97. Found: C, 44.72; H, 3.32; N, 11.84.

Selected X-ray structural data of **5**: C₂₇H₂₃Cl₃F₃IrN₆; *M* = 787.06; monoclinic; space group = *C*2/*c*, *a* = 29.4830(15) Å, *b* = 13.6321(7) Å, *c* = 14.3728(6) Å; β = 106.6523(16)°; *V* = 5534.4(5) Å³; *Z* = 8; ρ_{calcd} = 1.889 Mg·m⁻³; *F*(000) = 3056; crystal size = 0.256 × 0.064 × 0.033 mm³; *T* = 230 (2) K; μ = 5.165 mm⁻¹; 20902 reflections collected, 6356 independent reflections (*R*_{int} = 0.0322), max and min transmission = 0.7456 and 0.5699; restraints/parameters = 42/387,

GOF = 1.07, final $R_1[I > 2\sigma(I)] = 0.0312$ and wR_2 (all data) = 0.0885; largest diff peak and hole = 1.351 and $-1.005 \text{ e} \cdot \text{\AA}^{-3}$.

Preparation of $[\text{Ir}(\kappa^4\text{-N3C})\text{Cl}(\text{dmpzH})]$ (6). A mixture of 2 (500 mg, 0.40 mmol) and 3,5-dimethylpyrazole (dmpzH, 310 mg, 3.2 mmol) in 40 mL of DGME was refluxed for 14 h. After it cooled to RT, the solvent was removed and the residue was taken into CH_2Cl_2 , washed with water, dried over Na_2SO_4 , filtered, and concentrated to dryness. It was next purified by silica gel column chromatography (CH_2Cl_2 and ethyl acetate = 3:1) to afford light-yellow $[\text{Ir}(\kappa^4\text{-N3C})\text{Cl}(\text{dmpzH})]$ (6, 270 mg, 46%).

Spectral data of 6. ^1H NMR (400 MHz, CD_2Cl_2 , 298 K): δ 13.00 (br, NH, 1H), 8.94 (d, $J = 5.4$ Hz, 1H), 7.89–7.86 (m, 2H), 7.77 (t, $J = 7.8$ Hz, 1H), 7.48 (dd, $J = 8.0, 2.8$ Hz, 2H), 7.33 (d, $J = 8.0$ Hz, 1H), 7.16–7.12 (m, 1H), 7.01–6.99 (m, 2H), 6.90 (t, $J = 7.5$ Hz, 1H), 6.67 (t, $J = 7.2$ Hz, 1H), 5.96 (s, 1H), 2.67 (s, 3H), 2.56 (s, 3H), 0.87 (s, 3H). ^{19}F NMR (376 MHz, CD_2Cl_2 , 298 K): δ -60.85 (s, 3F). FD MS: m/z 716.1 ($\text{M} + \text{H}^+$). Anal. Calcd for $\text{C}_{27}\text{H}_{23}\text{ClF}_3\text{IrN}_6$: C, 45.28; H, 3.24; N, 11.73. Found: C, 45.45; H, 3.18; N, 11.61.

Preparation of $[\text{Ir}_2(\kappa^5\text{-N3C})(\text{mpz})_2(\text{CO})(\text{H})_2]$ (7). A mixture of 2 (50 mg, 0.04 mmol), 4-methylpyrazole (39 mg, 0.32 mmol) and K_2CO_3 (30 mg, 0.20 mmol) in 10 mL of DGME was refluxed for 12 h. After it cooled to RT, the solvent was removed and the residue was taken into excess of CH_2Cl_2 , washed with water, dried over Na_2SO_4 , filtered, and concentrated to dryness. It was next purified by silica gel column chromatography (CH_2Cl_2 and hexane = 1:2) to afford yellow $[\text{Ir}_2(\kappa^5\text{-N3C})(\text{mpz})_2(\text{CO})(\text{H})_2]$ (7, 16 mg, 41%).

Spectral data of 7. ^1H NMR (500 MHz, acetone- d_6 , 298 K): δ 8.29 (d, $J = 8.3$ Hz, 1H), 8.17 (td, $J = 7.8, 1.5$ Hz, 1H), 7.99 (t, $J = 7.9$ Hz, 1H), 7.93 (dd, $J = 8.0, 0.9$ Hz, 1H), 7.80–7.74 (m, 2H), 7.67 (s, 1H), 7.39 (d, $J = 7.3$ Hz, 1H), 7.27 (td, $J = 7.3, 1.1$ Hz, 1H), 7.24 (s, 1H), 7.20 (s, 1H), 6.93 (dd, $J = 7.6, 1.2$ Hz, 1H), 6.84 (td, $J = 8.3, 1.4$ Hz, 1H), 6.62 (td, $J = 7.3, 0.9$ Hz, 1H), 5.94 (s, 1H), 5.91 (s, 1H), 2.84 (s, 3H), 1.91 (s, 3H), 1.65 (s, 3H), -16.69 to -16.71 (m, 1H), -19.73 (d, $J = 8.6$ Hz, 1H). ^{19}F NMR (470 MHz, acetone- d_6 , 298 K): δ -58.20 (s, 3F). FD MS: m/z 968.1 ($\text{M} + \text{H}^+$). IR (νCO , KBr pellet): 2011 cm^{-1} . Anal. Calcd for $\text{C}_{31}\text{H}_{27}\text{F}_3\text{Ir}_2\text{N}_8\text{O}$: C, 38.42; H, 2.81; N, 11.56. Found: C, 38.71; H, 2.81; N, 11.33.

Selected X-ray structural data of 7: $\text{C}_{62.5}\text{H}_{55}\text{ClF}_6\text{Ir}_4\text{N}_{16}\text{O}_2$; $M = 1980.47$ monoclinic; space group = $P2_1/c$, $a = 20.6917(8) \text{ \AA}$, $b = 14.4421(5) \text{ \AA}$, $c = 22.1350(8) \text{ \AA}$; $\beta = 110.8392(8)^\circ$; $V = 6181.9(4) \text{ \AA}^3$; $Z = 4$; $\rho_{\text{calcd}} = 2.128 \text{ Mg} \cdot \text{m}^{-3}$; $F(000) = 3748$; crystal size = $0.130 \times 0.118 \times 0.066 \text{ mm}^3$; $T = 220(2) \text{ K}$; $\mu = 8.704 \text{ mm}^{-1}$; 45392 reflections collected, 14199 independent reflections ($R_{\text{int}} = 0.0365$), max and min transmission = 0.7456 and 0.6170; restraints/parameters = 22/860, GOF = 1.078, final $R_1[I > 2\sigma(I)] = 0.0296$ and wR_2 (all data) = 0.0633; largest diff peak and hole = 2.596 and $-2.481 \text{ e} \cdot \text{\AA}^{-3}$.

Preparation of $[\text{Ir}_2(\kappa^5\text{-N3C})(\text{dmpz})_2(\text{CO})(\text{H})_2]$ (8). A mixture of 2 (50 mg, 0.04 mmol), 3,5-dimethylpyrazole (30 mg, 0.32 mmol), and K_2CO_3 (30 mg, 0.20 mmol) in 10 mL of DGME was refluxed for 12 h. After it cooled to RT, the solvent was removed and the residue was taken into CH_2Cl_2 , washed with water, dried over Na_2SO_4 , filtered, and concentrated to dryness. It was next purified by silica gel column chromatography (CH_2Cl_2 and hexane = 1:2) to afford yellow $[\text{Ir}_2(\kappa^5\text{-N3C})(\text{dmpz})_2(\text{CO})(\text{H})_2]$ (8, 126 mg, 30%).

Spectral data of 8. ^1H NMR (500 MHz, acetone- d_6 , 298 K): δ 8.29 (d, $J = 8.3$ Hz, 1H), 8.16 (td, $J = 7.6, 1.5$ Hz, 1H), 8.02 (t, $J = 7.9$ Hz, 1H), 7.93 (d, $J = 7.8$ Hz, 1H), 7.88 (d, $J = 4.6$ Hz, 1H), 7.77 (d, $J = 8.0$ Hz, 1H), 7.40 (d, $J = 7.9$ Hz, 1H), 7.27 (t, $J = 6.1$ Hz, 1H), 7.22 (s, 1H), 7.09 (dd, $J = 7.4, 1.1$ Hz, 1H), 6.87 (td, $J = 7.1, 1.2$ Hz, 1H), 6.63 (t, $J = 7.3$ Hz, 1H), 5.77 (s, 1H), 5.42 (s, 1H), 2.85 (s, 3H), 2.52 (s, 3H), 2.13 (s, 3H), 0.43 (s, 3H), 0.17 (s, 3H), -16.65 to -16.67 (m, 1H), -19.75 (d, $J = 7.7$ Hz, 1H). ^{19}F NMR (470 MHz, acetone- d_6 , 298 K): δ -58.13 (s, 3F). FD MS: m/z 996.1 ($\text{M} + \text{H}^+$). IR (νCO , KBr pellet): 2007 cm^{-1} . Anal. Calcd for $\text{C}_{33}\text{H}_{31}\text{F}_3\text{Ir}_2\text{N}_8\text{O}$: C, 39.75; H, 3.13; N, 11.24. Found: C, 39.35; H, 3.31; N, 11.04.

X-ray Structural Determination. All crystals for X-ray diffraction were obtained from the slow evaporation of an acetonitrile solution at RT. Single crystal X-ray diffraction data were recorded on a Bruker D8 VENTURE diffractometer equipped with a Oxford Cryostream 800+ controller. The data collection was executed using

the SMART program. Cell refinement and data reduction were made with the SAINT program. The structure was determined using the SHELXTL/PC program and refined using full-matrix least-squares.⁵³ All non-hydrogen atoms were refined anisotropically, whereas all hydrogen atoms of hydrocarbyl fragments were placed at the calculated positions with fixed positional parameters, and hydride was independently located on the electron density map and included in the final stage of refinements. CCDC 1953441 (3), 1953442 (5) and 1953443 (7) contain the crystallographic data for this paper.

■ ASSOCIATED CONTENT

Supporting Information

The Supporting Information is available free of charge at <https://pubs.acs.org/doi/10.1021/acs.inorgchem.9b02799>.

General experimental procedures of all measurements and calculations, synthetic protocol of chelates, figures of normalized IR (νCO) spectra, TGA data curves, cyclic voltammograms, and ^1H NMR spectra, and tables of calculated energy levels and orbital transition analyses (PDF)

Accession Codes

CCDC 1953441–1953443 contain the supplementary crystallographic data for this paper. These data can be obtained free of charge via www.ccdc.cam.ac.uk/data_request/cif, or by emailing data_request@ccdc.cam.ac.uk, or by contacting The Cambridge Crystallographic Data Centre, 12 Union Road, Cambridge CB2 1EZ, UK; fax: +44 1223 336033.

■ AUTHOR INFORMATION

Corresponding Authors

*E-mail: apcslee@cityu.edu.hk.

*E-mail: yunchi@cityu.edu.hk.

ORCID

Chun-Sing Lee: 0000-0001-6557-453X

Yun Chi: 0000-0002-8441-3974

Notes

The authors declare no competing financial interest.

■ ACKNOWLEDGMENTS

This work was supported by the funding from Ministry of Science and Technology (MOST), featured areas research program within the framework of the Higher Education Sprout Project administrated by Ministry of Education (MOE) of Taiwan, and the Research Grant Council and City University of Hong Kong, Hong Kong SAR.

■ REFERENCES

- Xiao, L.; Chen, Z.; Qu, B.; Luo, J.; Kong, S.; Gong, Q.; Kido, J. Recent Progresses on Materials for Electrophosphorescent Organic Light-Emitting Devices. *Adv. Mater.* **2011**, *23*, 926–952.
- Xu, H.; Chen, R.; Sun, Q.; Lai, W.; Su, Q.; Huang, W.; Liu, X. Recent progress in metal–organic complexes for optoelectronic applications. *Chem. Soc. Rev.* **2014**, *43*, 3259–3302.
- Yang, X.; Zhou, G.; Wong, W.-Y. Functionalization of phosphorescent emitters and their host materials by main-group elements for phosphorescent organic light-emitting devices. *Chem. Soc. Rev.* **2015**, *44*, 8484–8575.
- Lu, C.-W.; Wang, Y.; Chi, Y. Metal Complexes with Azolate-Functionalized Multidentate Ligands: Tactical Designs and Optoelectronic Applications. *Chem. - Eur. J.* **2016**, *22*, 17892–17908.
- Henwood, A. F.; Zysman-Colman, E. Lessons learned in tuning the optoelectronic properties of phosphorescent iridium(III) complexes. *Chem. Commun.* **2017**, *53*, 807–826.

- (6) Ma, D.; Tsuboi, T.; Qiu, Y.; Duan, L. Recent Progress in Ionic Iridium(III) Complexes for Organic Electronic Devices. *Adv. Mater.* **2017**, *29*, 1603253.
- (7) Liao, J.-L.; Rajakannu, P.; Gnanasekaran, P.; Tsai, S.-R.; Lin, C.-H.; Liu, S.-H.; Chang, C.-H.; Lee, G.-H.; Chou, P.-T.; Chen, Z.-N.; Chi, Y. Luminescent Diiridium Complexes with Bridging Pyrazolates: Characterization and Fabrication of OLEDs Using Vacuum Thermal Deposition. *Adv. Opt. Mater.* **2018**, *6*, 1800083.
- (8) Li, T.-Y.; Wu, J.; Wu, Z.-G.; Zheng, Y.-X.; Zuo, J.-L.; Pan, Y. Rational design of phosphorescent iridium(III) complexes for emission color tunability and their applications in OLEDs. *Coord. Chem. Rev.* **2018**, *374*, 55–92.
- (9) Wei, Q.; Fei, N.; Islam, A.; Lei, T.; Hong, L.; Peng, R.; Fan, X.; Chen, L.; Gao, P.; Ge, Z. Small-Molecule Emitters with High Quantum Efficiency: Mechanisms, Structures, and Applications in OLED Devices. *Adv. Opt. Mater.* **2018**, *6*, 1800512.
- (10) Jacquemin, D.; Escudero, D. The short device lifetimes of blue PhOLEDs: insights into the photostability of blue Ir(III) complexes. *Chem. Sci.* **2017**, *8*, 7844–7850.
- (11) Williams, J. A. G.; Wilkinson, A. J.; Whittle, V. L. Light-emitting iridium complexes with tridentate ligands. *Dalton Trans* **2008**, 2081–2099.
- (12) Williams, J. A. G. The coordination chemistry of dipyritylbenzene: N-deficient terpyridine or panacea for brightly luminescent metal complexes? *Chem. Soc. Rev.* **2009**, *38*, 1783–1801.
- (13) Fleetham, T.; Wang, Z.; Li, J. Efficient deep blue electrophosphorescent devices based on platinum(II) bis(n-methylimidazolyl)benzene chloride. *Org. Electron.* **2012**, *13*, 1430–1435.
- (14) Chi, Y.; Chang, T.-K.; Ganesan, P.; Rajakannu, P. Emissive Bis-Tridentate Ir(III) Metal Complexes: Tactics, Photophysics and Applications. *Coord. Chem. Rev.* **2017**, *346*, 91–100.
- (15) Lin, J.; Wang, Y.; Gnanasekaran, P.; Chiang, Y.-C.; Yang, C.-C.; Chang, C.-H.; Liu, S.-H.; Lee, G.-H.; Chou, P.-T.; Chi, Y.; Liu, S.-W. Unprecedented Homoleptic Bis-Tridentate Iridium(III) Phosphors: Facile, Scaled-Up Production, and Superior Chemical Stability. *Adv. Funct. Mater.* **2017**, *27*, 1702856.
- (16) Adamovich, V.; Boudreault, P.-L. T.; Esteruelas, M. A.; Gómez-Bautista, D.; López, A. M.; Oñate, E.; Tsai, J.-Y. Preparation via a NHC Dimer Complex, Photophysical Properties, and Device Performance of Heteroleptic Bis(tridentate) Iridium(III) Emitters. *Organometallics* **2019**, *38*, 2738–2747.
- (17) Gnanasekaran, P.; Yuan, Y.; Lee, C.-S.; Zhou, X.; Jen, A. K. Y.; Chi, Y. Realization of Highly Efficient Red Phosphorescence from Bis-Tridentate Iridium(III) Phosphors. *Inorg. Chem.* **2019**, *58*, 10944–10954.
- (18) Huo, S.; Carroll, J.; Vezzu, D. A. K. Design, Synthesis, and Applications of Highly Phosphorescent Cyclometalated Platinum Complexes. *Asian J. Org. Chem.* **2015**, *4*, 1210–1245.
- (19) Fleetham, T. B.; Huang, L.; Klimes, K.; Brooks, J.; Li, J. Tridentate Pt(II) complexes with 6-membered chelate rings: A new route for stable and efficient blue OLEDs. *Chem. Mater.* **2016**, *28*, 3276–3282.
- (20) Wang, X.; Peng, T.; Nguyen, C.; Lu, Z.-H.; Wang, N.; Wu, W.; Li, Q.; Wang, S. Highly Efficient Deep-Blue Electrophosphorescent Pt(II) Compounds with Non-Distorted Flat Geometry: Tridentate versus Macrocyclic Chelate Ligands. *Adv. Funct. Mater.* **2017**, *27*, 1604318.
- (21) Li, G.; Zhu, Z.-Q.; Chen, Q.; Li, J. Metal complex based delayed fluorescence materials. *Org. Electron.* **2019**, *69*, 135–152.
- (22) Wang, X.; Wang, S. Phosphorescent Pt(II) Emitters for OLEDs: From Triarylboron-Functionalized Bidentate Complexes to Compounds with Macrocyclic Chelating Ligands. *Chem. Rec.* **2019**, *19*, 1693–1709.
- (23) Kashif, M. K.; Axelson, J. C.; Duffy, N. W.; Forsyth, C. M.; Chang, C. J.; Long, J. R.; Spiccia, L.; Bach, U. A New Direction in Dye-Sensitized Solar Cells Redox Mediator Development: In-Situ Fine-Tuning of the Cobalt(II)/(III) Redox Potential through Lewis Base Interactions. *J. Am. Chem. Soc.* **2012**, *134*, 16646.
- (24) Whited, M. T.; Mankad, N. P.; Lee, Y.; Oblad, P. F.; Peters, J. C. Dinitrogen Complexes Supported by Tris(phosphino)silyl Ligands. *Inorg. Chem.* **2009**, *48*, 2507–2517.
- (25) Rossin, A.; Gutsul, E. I.; Belkova, N. V.; Epstein, L. M.; Gonsalvi, L.; Lledós, A.; Lyssenko, K. A.; Peruzzini, M.; Shubina, E. S.; Zanobini, F. Mechanistic Studies on the Interaction of $[(\kappa^3\text{-P,P,P-NP}_3)\text{IrH}_3]$ $[\text{NP}_3 = \text{N}(\text{CH}_2\text{CH}_2\text{PPh}_2)_3]$ with HBF_4 and Fluorinated Alcohols by Combined NMR, IR, and DFT Techniques. *Inorg. Chem.* **2010**, *49*, 4343–4354.
- (26) Takeda, N.; Watanabe, D.; Nakamura, T.; Unno, M. Synthesis and Complexation of a New Tripodal Tetradentate Ligand, a Silyl Ligand Tethered with Three Thioether Moieties. *Organometallics* **2010**, *29*, 2839–2841.
- (27) Gloaguen, Y.; Jongens, L. M.; Reek, J. N. H.; Lutz, M.; de Bruin, B.; van der Vlugt, J. I. Reductive Elimination at an Ortho-Metalated Iridium(III) Hydride Bearing a Tripodal Tetrakisphosphorus Ligand. *Organometallics* **2013**, *32*, 4284–4291.
- (28) Corona-González, M. V.; Zamora-Moreno, J.; Cuevas-Chávez, C. A.; Rufino-Felipe, E.; Mothes-Martin, E.; Coppel, Y.; Muñoz-Hernández, M. A.; Vendier, L.; Flores-Alamo, M.; Grellier, M.; Sabo-Etienne, S.; Montiel-Palma, V. A family of rhodium and iridium complexes with semirigid benzylsilyl phosphines: from bidentate to tetradentate coordination modes. *Dalton Trans* **2017**, *46*, 8827–8838.
- (29) Koren, K.; Borisov, S. M.; Saf, R.; Klimant, I. Strongly Phosphorescent Iridium(III)–Porphyrins – New Oxygen Indicators with Tuneable Photophysical Properties and Functionalities. *Eur. J. Inorg. Chem.* **2011**, *2011*, 1531–1534.
- (30) Chen, D.; Li, K.; Guan, X.; Cheng, G.; Yang, C.; Che, C.-M. Luminescent Iridium(III) Complexes Supported by a Tridentate Trianionic Ligand Scaffold with Mixed O, N, and C Donor Atoms: Synthesis, Structures, Photophysical Properties, and Material Applications. *Organometallics* **2017**, *36*, 1331–1344.
- (31) Li, Y.-S.; Liao, J.-L.; Lin, K.-T.; Hung, W.-Y.; Liu, S.-H.; Lee, G.-H.; Chou, P.-T.; Chi, Y. Sky Blue-Emitting Iridium(III) Complexes Bearing Nonplanar Tridentate Chromophore and Bidentate Ancillary. *Inorg. Chem.* **2017**, *56*, 10054–10060.
- (32) DeRosa, M. C.; Mosher, P. J.; Yap, G. P. A.; Focsaneanu, K.-S.; Crutchley, R. J.; Evans, C. E. B. Synthesis, Characterization, and Evaluation of $[\text{Ir}(\text{ppy})_2(\text{vpy})\text{Cl}]$ as a Polymer-Bound Oxygen Sensor. *Inorg. Chem.* **2003**, *42*, 4864–4872.
- (33) Li, J.; Djurovich, P. I.; Alleyne, B. D.; Tsyba, I.; Ho, N. N.; Bau, R.; Thompson, M. E. Synthesis and characterization of cyclometalated Ir(III) complexes with pyrazolyl ancillary ligands. *Polyhedron* **2004**, *23*, 419–428.
- (34) Baranoff, E.; Jung, I.; Scopelliti, R.; Solari, E.; Grätzel, M.; Nazeeruddin, M. K. Room-temperature combinatorial screening of cyclometalated iridium(III) complexes for a step towards molecular control of colour purity. *Dalton Trans* **2011**, *40*, 6860–6867.
- (35) Chandrasekhar, V.; Mahanti, B.; Bandipalli, P.; Bhanuprakash, K. Cyclometalated Iridium(III) Complexes Containing Hydroxide/Chloride Ligands: Isolation of Heterobridged Dinuclear Iridium(III) Compounds Containing $\mu\text{-OH}$ and $\mu\text{-Pyrazole}$ Ligands. *Inorg. Chem.* **2012**, *51*, 10536–10547.
- (36) Alam, P.; Kaur, G.; Sarmah, A.; Roy, R. K.; Choudhury, A. R.; Laskar, I. R. Highly Selective Detection of H^+ and OH^- with a Single-Emissive Iridium(III) Complex: A Mild Approach to Conversion of Non-AIEE to AIEE Complex. *Organometallics* **2015**, *34*, 4480–4490.
- (37) Coe, B. J.; Helliwell, M.; Raftery, J.; Sánchez, S.; Peers, M. K.; Scrutton, N. S. Cyclometalated Ir(III) complexes of deprotonated N-methylbipyridinium ligands: effects of quaternised N centre position on luminescence. *Dalton Trans* **2015**, *44*, 20392–20405.
- (38) Bushnell, G. W.; Fjeldsted, D. O. K.; Stobart, S. R.; Zaworotko, M. J.; Knox, S. A. R.; MacPherson, K. A. Pyrazolyl-bridged iridium dimers. 7. Synthesis and properties of analogs of $[\text{Ir}(\text{COD})(\mu\text{-pz})]_2$ ($\text{pzH} = \text{pyrazole}$), $[\text{Ir}_2(\text{COD})_2(\mu\text{-pz})(\mu\text{-fpz})]$ ($\text{fpzH} = 3,5\text{-bis}(\text{trifluoromethyl})\text{pyrazole}$) and $[\text{IrRh}(\text{COD})_2(\mu\text{-pz})_2]$. Crystal and molecular structures of bis(cyclooctadiene)bis($\mu\text{-3-phenyl-5-methylpyrazolyl}$)diiridium(I) (disymmetric isomer) and bis-

(cycloocta-1,5-diene)bis(μ -3,4,5-trimethylpyrazolyl)diiridium(I). *Organometallics* **1985**, *4*, 1107–1114.

(39) Carmona, D.; Oro, L. A.; Lamata, M. P.; Puebla, M. P.; Ruiz, J.; Maitlis, P. M. Binuclear rhodium and iridium complexes containing pentamethylcyclopentadienyl and pyrazolate ligands. *J. Chem. Soc., Dalton Trans.* **1987**, 639–645.

(40) Yuan, Y.; Jiménez, M. V.; Sola, E.; Lahoz, F. J.; Oro, L. A. Sequential C–H Activation and Dinuclear Insertion of Ethylene Promoted by a Diiridium Complex. *J. Am. Chem. Soc.* **2002**, *124*, 752–753.

(41) Ma, B.; Li, J.; Djurovich, P. I.; Yousufuddin, M.; Bau, R.; Thompson, M. E. Synthetic Control of Pt–Pt Separation and Photophysics of Binuclear Platinum Complexes. *J. Am. Chem. Soc.* **2005**, *127*, 28–29.

(42) Hsieh, H.-Y.; Lin, C.-H.; Tu, G.-M.; Chi, Y.; Lee, G.-H. Platinum(II) complexes with spatially encumbered chelates; syntheses, structure and photophysics. *Inorg. Chim. Acta* **2009**, *362*, 4734–4739.

(43) Rachford, A. A.; Castellano, F. N. Thermochromic Absorption and Photoluminescence in [Pt(ppy)(μ -Ph₂pz)]₂. *Inorg. Chem.* **2009**, *48*, 10865–10867.

(44) Chakraborty, A.; Deaton, J. C.; Haefele, A.; Castellano, F. N. Charge-Transfer and Ligand-Localized Photophysics in Luminescent Cyclometalated Pyrazolate-Bridged Dinuclear Platinum(II) Complexes. *Organometallics* **2013**, *32*, 3819–3829.

(45) Zhou, C.; Tian, Y.; Yuan, Z.; Han, M.; Wang, J.; Zhu, L.; Tameh, M. S.; Huang, C.; Ma, B. Precise Design of Phosphorescent Molecular Butterflies with Tunable Photoinduced Structural Change and Dual Emission. *Angew. Chem., Int. Ed.* **2015**, *54*, 9591–9595.

(46) Brown-Xu, S. E.; Kelley, M. S. J.; Fransted, K. A.; Chakraborty, A.; Schatz, G. C.; Castellano, F. N.; Chen, L. X. Tunable Excited-State Properties and Dynamics as a Function of Pt–Pt Distance in Pyrazolate-Bridged Pt(II) Dimers. *J. Phys. Chem. A* **2016**, *120*, 543–550.

(47) Arnal, L.; Fuertes, S.; Martín, A.; Baya, M.; Sicilia, V. A Cyclometalated N-Heterocyclic Carbene: The Wings of the First Pt₂(II,II) Butterfly Oxidized by CHI₃. *Chem. - Eur. J.* **2018**, *24*, 18743–18748.

(48) Carmona, E.; Paneque, M.; Santos, L. L.; Salazar, V. Iridium carboxycarbene complexes by CH bond activation of aliphatic ethers and of alkyl aryl ethers. *Coord. Chem. Rev.* **2005**, *249*, 1729–1735.

(49) Ward, M. D.; McCleverty, J. A.; Jeffery, J. C. Coordination and supramolecular chemistry of multinucleating ligands containing two or more pyrazolyl-pyridine 'arms'. *Coord. Chem. Rev.* **2001**, *222*, 251–272.

(50) Slugovc, C.; Padilla-Martinez, I.; Sirol, S.; Carmona, E. Rhodium- and iridium-trispyrazolylborate complexes: C-H activation and coordination chemistry. *Coord. Chem. Rev.* **2001**, *213*, 129–157.

(51) Chiu, Y.-C.; Lin, C.-H.; Hung, J.-Y.; Chi, Y.; Cheng, Y.-M.; Wang, K.-W.; Chung, M.-W.; Lee, G.-H.; Chou, P.-T. Authentic-Blue Phosphorescent Iridium(III) Complexes Bearing Both Hydride and Benzyl Diphenylphosphine; Control of the Emission Efficiency by Ligand Coordination Geometry. *Inorg. Chem.* **2009**, *48*, 8164–8172.

(52) Liao, J.-L.; Devereux, L. R.; Fox, M. A.; Yang, C.-C.; Chiang, Y.-C.; Chang, C.-H.; Lee, G.-H.; Chi, Y. Role of the Diphosphine Chelate in Emissive, Charge-Neutral Iridium(III) Complexes. *Chem. - Eur. J.* **2018**, *24*, 624–635.

(53) Sheldrick, G. M. Crystal structure refinement with SHELXL. *Acta Crystallogr., Sect. C: Struct. Chem.* **2015**, *71*, 3–8.